2.8-Å-Resolution Crystal Structure of an Active-Site Mutant of Aspartate Aminotransferase from *Escherichia coli*[†,‡]

Douglas L. Smith,[§,∥] Steven C. Almo,[§,⊥] Michael D. Toney,[#] and Dagmar Ringe*[,§]

Department of Chemistry, Massachusetts Institute of Technology, Cambridge, Massachusetts 02139, Committee on Higher Degrees in Biophysics, Harvard University, Cambridge, Massachusetts 02138, and Biochemistry Department, University of California at Berkeley, Berkeley, California 94720

Received March 8, 1989

ABSTRACT: The three-dimensional structure of a mutant of the aspartate aminotransferase from *Escherichia coli*, in which the active-site lysine has been substituted by alanine (K258A), has been determined at 2.8-Å resolution by X-ray diffraction. The mutant enzyme contains pyridoxamine phosphate as cofactor. The structure is compared to that of the mitochondrial aspartate aminotransferase. The most striking differences, aside from the absence of the lysine side chain, occur in the positions of the pyridoxamine group and of tryptophan 140.

Enzymatic transamination was discovered 50 years ago (Braunstein & Kritzman, 1937). Since then, more than 60 transaminases have been identified, differing in substrate specificity and capable of transforming over 100 amino acids including D amino acids and ω amino acids (Cooper & Meister, 1985; John & Fowler, 1985). The best characterized of these is aspartate aminotransferase [AATase[1] (EC 2.6.1.1)], whose properties have been reviewed by Braunstein (1973) and Jansonius and Vincent (1987). The essential cofactor in these reactions is pyridoxal phosphate (PLP, a vitamin B_6 derivative), which is bound covalently through an azomethine linkage between its C-4′ carbon atom and the ε-amino group of an active-site lysine. The aspartate aminotransferase reaction involves a double displacement (ping-pong Bi Bi) (Snell, 1945; Metzler & Snell, 1952; Velick & Vavra, 1962; Kiick & Cook, 1983), in which the enzyme shuttles between the pyridoxal phosphate form (PLP) and the pyridoxamine phosphate form (PMP).

L-aspartate or L-glutamate + PLP–enzyme ↔ PMP–enzyme + oxaloacetate or ketoglutarate

Conformational changes occur during the course of the reaction (Birchmeier et al., 1973; Gehring & Christen, 1978), and various coenzyme–substrate intermediates have been identified by characteristic absorption and circular dichroism spectra (Braunstein, 1973; Metzler, 1979). The three-dimensional structures of several vertebrate isozymes and various derivatives are available (Ford et al., 1980; Borisov et al., 1980; Arnone et al., 1985; Harutyunyan et al., 1982; Torchinsky et al., 1982). This information has been molded into a detailed proposal for the mechanism of action of this enzyme (Kirsch et al., 1984; Jansonius & Vincent, 1987).

Aspartate aminotransferase from *Escherichia coli* has been cloned, sequenced, and expressed (Malcolm & Kirsch, 1985). The protein sequence of the *E. coli* enzyme has been determined (Kondo et al., 1984). Sequence homology with the avian and mammalian isozymes is 40%. The enzyme is an α_2 dimer of 2 × 396 amino acids ($M_r \sim 88\,000$) in which the active-site residues are identical with their eukaryotic counterparts. The earlier determined structures were thus used to guide the site-specific mutagenesis studies on *E. coli* AATase until the latter structure became available (Smith et al., 1986). We now report the crystal structure of a site-specific mutant of *E. coli* aspartate aminotransferase at 2.8-Å resolution.

The mutant reported here is one in which lysine 258, which forms the Schiff base with the pyridoxal phosphate, has been changed to alanine. The enzyme still binds PLP and PMP, but not covalently. The PMP form of the enzyme forms a covalent stable ketimine with α-ketoglutarate and effects a β-decarboxylation of oxalacetate, followed by transamination of the bound three-carbon product to give the PLP–aldimine of alanine as final product (Kirsch et al., 1987).

Materials and Methods

(*a*) *Preparation of Enzyme and Crystallization.* Samples of the mutant enzyme, isolated and purified in the manner described earlier (Malcolm & Kirsch, 1985; Smith et al., 1986) for the wild-type enzyme, were furnished by W. L. Finlayson and Professor J. F. Kirsch, University of California, Berkeley. Crystals of the mutant grew readily by batch methods from a 5.2 mg/mL protein solution in 50 mM potassium phosphate buffer (pH 7.5) containing 53% saturated ammonium sulfate. Crystals as large as 2 mm × 0.5 mm × 0.3 mm grew as colorless prisms at room temperature within a week. Crystals of the wild-type enzyme inhibited with succinate have also been reported (Kamitori et al., 1987).

Isomorphous heavy-atom derivatives were prepared by soaking crystals for 24 and 48 h, respectively, in 1 mM solu-

[†] This project was supported, in part, by a grant from the W. R. Grace Co. (to D.R.). The work at Berkeley was supported by NIH Grant GM 35393 (to J. Kirsch). This paper is dedicated to Greg Petsko on the occasion of his thirty-ninth birthday.

[‡] The atomic coordinates in this paper have been submitted to the Brookhaven Protein Data Bank under Identification Code 2AAT.

* Author to whom correspondence should be addressed.
[§] Massachusetts Institute of Technology.
[∥] Present address: Eastman Kodak Co., Rochester, NY 14650.
[⊥] Harvard University.
[#] University of California at Berkeley.

[1] Abbreviations: AATase, aspartate aminotransferase; PMP, pyridoxamine phosphate; PLP, pyridoxal phosphate. The residue numbering used in this paper has been chosen to maximize homology between the *E. coli* and chicken mitochondrial AATase.

0006-2960/89/0428-8161$01.50/0

Table I: Lattice Constants for *E. coli* AATases

derivative	*a*	*b*	*c*	no. of crystals	method
native	156.80 (4)[a]	86.74 (4)	79.84 (6)	5	diffractometer
DMA	156.74 (5)	86.85 (4)	79.59 (4)	4	diffractometer
PTCN	157.18 (5)	87.20 (6)	79.46 (1)	3	diffractometer
EMP	157.4	86.7	79.8	1	precession

[a] The errors are standard deviations expressed in terms of the least significant digit. For native, DMA, and PTCN, the standard deviations were calculated from the deviations of the multiple determinations: $\sigma^2(a_{av}) = \sum_{i=1}^{n}[(a_{av} - a_i)^2/[n(n-1)]]$.

tions of dimercury acetate (DMA) and $K_2Pt(CN)_4$ (PTCN) in a buffered mother liquor (pH 7.5) of 40 mM potassium phosphate, 60% saturated ammonium sulfate, 20 μM pyridoxamine 5′-phosphate (PMP), and 1 mM sodium azide. A third derivative resulted from soaking crystals for 24 h in 0.3 mM ethylmercury phosphate (EMP) in a 50 mM Tris·HCl buffer (pH 7.0) with 60% saturated ammonium sulfate. A fourth derivative was prepared from *p*-(chloromercuri)benzoate but was not used because of the similarity of its diffraction pattern to that of the DMA derivative.

(*b*) *Characterization of the Crystals.* Precession photographs showed that crystals of the mutant and heavy-atom derivatives are isomorphous. They are orthorhombic with $C222_1$ symmetry. The lattice constants are given in Table I and are identical with those previously reported by us for the wild-type enzyme (Smith et al., 1986).

The mutant enzyme has 396 amino acid residues with a molecular mass of 43 516 daltons (Kondo et al., 1984). The total molecular mass, including the cofactor, is 43 749 daltons. There are four dimers per unit cell and one subunit in the asymmetric unit. V_m, the volume per unit mass, is 3.1 Å^3 dalton, as found to be typical for protein crystals (Matthews, 1968).

(*c*) *X-ray Studies.* X-ray diffraction data were obtained with Ni-filtered Cu Kα radiation from sealed tube generators at 20 °C with crystals averaging 1.1 mm × 0.3 mm × 0.25 mm in size. Data for the native mutant and the DMA and PTCN derivatives were collected on a Nicolet P3 diffractometer. Data for the EMP derivative were taken on CRAD (Crystallographic Area Detector), a prototypic crystal data collection system employing a spherical area proportional detector (Bolon et al., 1981). Initial attempts to collect data at 0 °C with the wild-type enzyme had resulted in rapid crystal deterioration, caused possibly by a phase transition upon cooling, and therefore all further experiments were done at ambient room temperature. We elected to solve the crystal structure of the Lys 258 to alanine mutant (K258A) first, rather than that of the wild-type enzyme, because the mutant protein consistently yielded crystals of superior size and diffracting quality.

Reflections for two native crystals were measured to 2.8-Å resolution by the background–peak–background method. An empirical absorption curve for each crystal (North et al., 1968) was used to correct for absorption effects. Crystal decay was monitored by five check reflections remeasured after every 300 reflections. The observed decay rate was linear and was corrected for as a function of time with values of 40% and 50% damage for the two crystals used.

Only reflections with background-corrected intensities greater than one standard deviation (on the basis of counting statistics) were processed. After correction for absorption, decay, and Lorentz-polarization effects, the structure factors from the two crystals were scaled by using reflections in an overlapping shell. The merging agreement factor was 15% on intensities. The final data set included 8783 unique reflections, 64% of the theoretical number expected to 2.8-Å resolution.

Diffraction data, including Friedel pairs, were measured with Wyckoff scans (Wyckoff, 1985) for the DMA and PTCN derivatives. The two reflections of the Friedel pair were collected close in time to minimize differences in radiation damage between the measurements. Absorption and radiation decay were monitored as for the native crystals. The decay rates for the two derivatives were linear. Two DMA crystals (maximum decay 60% and 55%) and three PTCN crystals (maximum decay 45%, 35%, and 27%) were used to collect data to 3.0-Å resolution. Only reflections with background-corrected intensities greater than one standard deviation for DMA and two standard deviations for PTCN were processed. After absorption, decay, and Lorentz-polarization effects were corrected for, the structure factors for the crystals of each derivative were scaled by overlapping reflections and merged together with agreement factors of 8.8% for DMA and 8.9% for PTCN. The final data sets included 7710 (DMA; 64% of theoretical) and 7010 (PTCN; 60% of theoretical) matching reflections to 3.0-Å resolution.

Only one crystal of the EMP derivative was needed to collect data on CRAD. The crystal was aligned on a precession camera with its *c* axis along the rotation axis (φ). One goniometer head arc was offset by 30° to remove the symmetry axis from the rotation axis, thereby minimizing the effect of the blind area inherent in all rotation methods. Data were collected in 1080 frames distributed over 135° on φ (8 frames/deg) for 2 min/frame. To monitor crystal decay, 40 check frames were remeasured every 200 frames for 1 min/frame. A 2.4-Å resolution data set with up to 8-fold redundancy was collected in approximately 44 h. The presence of 1057 useable reflections in the check frames allowed the decay to be modeled as a function of time (*t*) and of resolution (*a*). The correction was applied as $I_{corr} = I_{obs}/(1 - at)$ for nine resolution shells. The maximum decay ranged from 5% at low resolution to 45% for the 3.4–2.4-Å shell and dramatically shows the importance of the use of a resolution-dependent model for decay corrections. No absorption correction was made. Equivalent reflections were averaged (merging R = 13% on I), but the Friedel differences were retained. Only reflections with net intensities greater than 1.5 standard deviations were processed. The final data set included 8443 (63%) reflections matched to native reflections to 2.8 Å.

The derivative data were scaled to the native data in blocks of reciprocal space. The resulting mean fractional isomorphous differences for the derivatives were 0.18 (DMA), 0.15 (PTCN), and 0.23 (EMP).

(*d*) *Structure Determination.* The heavy-atom positions for the DMA derivative were determined from isomorphous, anomalous, and F_{HLE} (Dodson & Vijayan, 1971) difference Patterson maps. In addition, the F_{HLE}'s for the DMA derivative were used in the direct phasing program MULTAN (Germain et al., 1971). The solution with the third highest combined figure of merit confirmed the mercury positions found previously for this derivative by Patterson synthesis and showed no further sites. The good quality of the DMA and native data was evident after the application of the iterative single isomorphous replacement method for phase determination (Wang, 1985). The procedure suggested by Wang resulted in an average figure of merit of 0.73 and agreement factor R = 0.27. More importantly, the resulting 3-Å protein

Table II: Heavy-Atom Parameters from Refinement

derivative	fractional coordinates					
	x	y	z	B (Å^2)	occ[a]	$R(F_{HLE})$[b]
DMA						
site 1	0.8666	0.5453	0.7961	19	0.81	0.57
site 2	0.9249	0.6415	0.3008	42	0.72	
site 3	0.9021	0.8696	0.8762	49	0.66	
EMP						
site 1	0.8542	0.5144	0.8460	29	0.98	0.73
site 2	0.9218	0.6318	0.2894	25	0.42	
site 3	0.9009	0.8686	0.8737	40	0.70	
site 4	0.9222	0.6507	0.3166	48	0.46	
PTCN						
site 1	0.9645	0.3163	0.1753	38	0.40	0.58
site 2	0.8550	0.3520	0.3798	21	0.39	
site 3	0.8006	0.2976	0.2961	31	0.52	
site 4	0.8178	0.3150	0.3309	44	0.31	

[a] Relative occupancies adjusted by the scale factor from Hendrickson–Konnert refinement of the protein structure. [b] $R(F_{HLE}) = \sum|F_{HLE} - F_{HCALC}|/F_{HLE}$, where F_{HLE} is an estimate of F_H, the heavy-atom structure factor, from combined isomorphous and anomalous differences (Dodson & Vijayan, 1971).

map clearly shows the enzyme boundaries and a considerable amount of the secondary structure. The dimeric nature of the enzyme, with the dimer lying on a crystallographic 2-fold axis along a, was confirmed.

The heavy-atom positions for the PTCN and EMP derivatives were determined from difference Fourier maps calculated by using DMA phases and the relevant heavy-atom-derivative structure factors. These heavy-atom positions were subsequently confirmed from isomorphous difference Patterson syntheses. Least-squares adjustment (Terwilliger & Eisenberg, 1983) of position, occupancy, and temperature factor for each heavy-atom site using isomorphous differences for all three derivatives and isomorphous plus anomalous differences for the DMA and EMP derivatives gave the refined parameters given in Table II.

Centroid phase angles from the heavy-atom refinement of all three derivatives were then used to calculate a 3-Å multiple isomorphous replacement protein map on a 1-Å grid sectioned along a. The overall figure of merit for the phases calculated from all three derivatives was 0.75. The entire polypeptide chain was readily traced by using the published chicken mitochondrial AATase structure (Ford et al., 1980) as a guide. Although there is only 40% homology between the two enzymes, the secondary and tertiary structures are very similar. This preliminary α-carbon backbone structure included the positions of 355 residues.

The polypeptide chain was adjusted by using the program FRODO (Jones, 1982) with an Evans and Sutherland PS300 graphics system linked to a Digital Equipment Corp. VAX 11/750 computer. The α-carbon chain was carefully refitted to the electron density, expanding the chain to 398 residues. The next stage was the transformation of the α-carbon structure to polyalanine by matching fragments from a standard library of highly refined protein structures to segments of the chain by use of the DGLP feature of FRODO (Jones & Thirup, 1986). This step resulted in a 394-residue polyalanine model.

Finally, by use of the structure of the chicken mitochondrial AATase (Ford et al., 1980), the sequence alignment of the *E. coli* enzyme (Kondo et al., 1984), and the side-chain electron densities, the entire sequence of 396 amino acids was substituted for the polyalanine sequence. In this process, 18 residues were deleted and 16 inserted in the electron density of the chain, an error rate of almost 10% for the polyalanine fitting. In addition, a PMP coenzyme molecule was clearly evident and easily positioned. One remaining prominent electron density feature in the active site was attributed to a sulfate ion.

Table III: Results of Least-Squares Refinement

no. of cycles	56
final R factor [$= \sum(\|F_o\| - \|F_c\|)/\sum\|F_o\|$]	0.22
no. of reflections (10.0–2.8 Å)	8433
no. of atoms (non-hydrogen, no solvent)	3086
no. of variable parameters	9260
restraints applied	
σ (bond length, Å)	0.020
σ (angle length, Å)	0.060
σ (planar distance, Å)	0.070
deviations observed[a]	
rms Δ (bond length, Å)	0.009
rms Δ (angle length, Å)	0.071
rms Δ (planar distance, Å)	0.064
overall B factor, Å^2	14

[a] These Δ values are root-mean-square (rms) deviations from the corresponding values for ideal groups derived from small-molecule structural studies (Sielecki et al., 1979).

The full structure was subjected to the constrained least-squares parameter optimization procedure of Hendrickson and Konnert (1980). The starting R factor was 40% for all data from 10- to 3.5-Å resolution (Table III). During the course of the refinement, the structure was adjusted manually twice from $2F_o - F_c$ maps to improve the fit of model to electron density. Significant changes included assignment of two proline residues (Pro 138 and Pro 195) to a cis configuration. These two prolines have also been assigned a cis configuration in the mitochondrial AATase (Jansonius et al., 1985). Refinement allowed the extension of phase determination from 3- to 2.8-Å resolution. The final R factor is 22% for all data from 10- to 2.8-Å resolution, with very good stereochemistry (rms deviation in bond length from ideality of 0.009 Å). The structure has also been refined, independently, by a new refinement method using molecular dynamics (Brünger et al., 1987). Molecular dynamics refinement reduced the R factor from 40% to 22.6% with equally good geometry, without any manual rebuilding (Brünger, 1988). During this molecular dynamics refinement, Pro 138 automatically flipped from trans to cis.

Finally, a difference electron density map was calculated between the K258A mutant data and the wild-type data by using the refined phase angles for the mutant structure.

Results and Discussion

The overall shapes of the *E. coli* mutant AATase subunit and dimer structures are the same as those observed for the mitochondrial AATase (Kirsch et al., 1984) and for the wild-type *E. coli* AATase (D. L. Smith, unpublished results). However, there are some differences between the *E. coli* and mitochondrial isozymes: (1) The polypeptide chain of the *E. coli* enzyme is five residues shorter than that of the mitochondrial enzyme. (2) Lysine 258 is not present in the mutant, so some differences in the binding of the PMP are observed. (3) There is a sulfate ion in the active site that is not in the structure of the mitochondrial enzyme. The comparisons reported here are primarily between the PLP form of mitochondrial AATase at 2.3-Å resolution, because these refined coordinates are available (J. N. Jansonius, private communication), and the PMP form of the K258A mutant enzyme from *E. coli*. The PMP-containing structure at 2.8 Å has been reported for the mitochondrial enzyme (Kirsch et al., 1984), but these coordinates are not yet available. The wild-type *E. coli* AATase structure is not yet refined at high resolution.

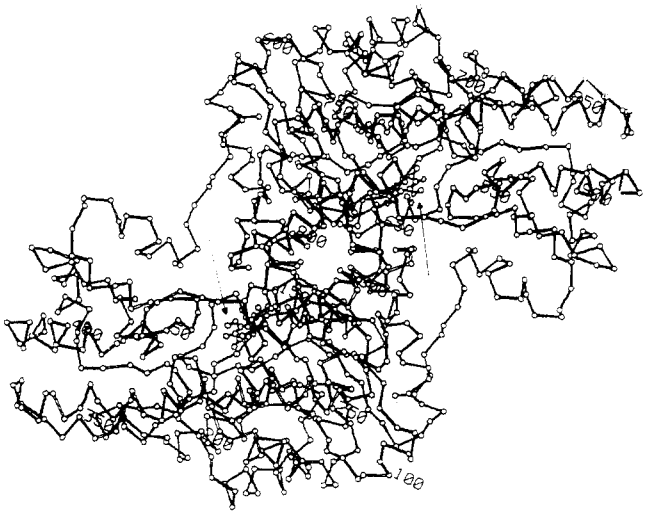

FIGURE 1: α-Carbon tracing of the dimer of the K258A mutant of *E. coli* AATase. The view is down the molecular 2-fold axis. The lower subunit is shown in open bonds and numbered from 1 to 405; the upper subunit is shown in filled bonds and numbered from 500 to 905. The active site in both subunits is indicated by the presence of the PMP structure (arrow). The numbering, which follows the convention used for the mitochondrial AATase, is based on maximum overlap of homologous sequences and reflects some insertions and deletions.

The complete structure of the AATase enzyme consists of two subunits (Figure 1), each with two domains (Figure 2): a large one containing the lysine (K258) that forms the Schiff base with the PLP in the wild-type enzyme and a small one that interacts with the α-carboxyl group of the substrate when it is bound. The large domain of one subunit also contains the specificity site for the distal-carboxyl group of the substrate when it is bound to the other subunit. These two domains are connected by a 46-Å helix (Figure 2). These two domains in the mitochondrial enzyme have an "open" configuration in the unliganded enzyme, which is closed upon association with inhibitors such as maleate or α-methyl aspartate (Jansonius & Vincent, 1987). This same type of domain movement has been observed in the cytosolic enzyme (Arnone et al., 1985). The structure of the K258A mutant of *E. coli* AATase appears to be between those of the open and closed forms observed for the mitochondrial enzyme. Each domain can be fitted to its analogous domain in the mitochondrial enzyme individually, with a 1.1-Å rms deviation of backbone atoms. However, when the overlap of the large domains is maximized, the small domain must be rotated by 10° toward the active site around an axis perpendicular to the long helix to maximize the overlap of the backbone atoms. The rotation necessary to obtain the closed from from the open form of the mitochondrial enzyme is 13° around the same axis and was interpreted as a conformational change accompanying the binding of specific inhibitors (Kirsch et al., 1984). Thus, the presence of the sulfate ion, a competitive inhibitor of this enzyme, in the active site may influence the tertiary structure of the mutant enzyme.

The tertiary structure of the K258A mutant enzyme is practically identical with those of the mitochondrial enzyme and the wild-type AATase from *E. coli*, with the exception noted above. The characteristic features of the monomer consist of the large coenzyme binding domain, the small domain, and an extended N-terminal arm, the end of which interacts with the other subunit (Figure 1). The large domain is composed of a seven-stranded mixed (six parallel, one antiparallel) pleated sheet incorporated in an α/β structure and the N-terminal end of the long helix. The striking secondary structural features of the small domain are four parallel helices, a small segment of mixed pleated sheet, and the C-terminal end of the long helix. Most of the deletions that occur in the bacterial relative to the mitochondrial isozyme occur in helices and at the N-terminus. However, the main features of the infrastructure of β-sheet and α-helices are not changed as a consequence. There is no significant change in secondary or tertiary structure due to the absence of the lysine 258 side chain.

The active site of AATase K258A can be described in terms of five regions, each with specific interactions (Figure 3). The position of the substrate is stabilized primarily by interactions of the α- and distal-carboxylate groups with Arg 386 (in the small domain) and Arg 292 (in the large domain of the other subunit of the dimer), respectively. These assignments are based on the structure of the mitochondrial enzyme inhibited with α-methyl aspartate (Jansonius & Vincent, 1987). Both of these residues are conserved in both isozymes. The positions of these two residues are superimposable in the mutant and wild-type enzymes. The phosphate group of the cofactor is stabilized by the same interactions in the *E. coli* enzyme as in the mitochondrial enzyme, with one exception. The group is situated at the N-terminus of the helix formed by residues 108–122. A network of hydrogen bonds originating from the neighboring residues includes the side-chain OH's of Ser 255,

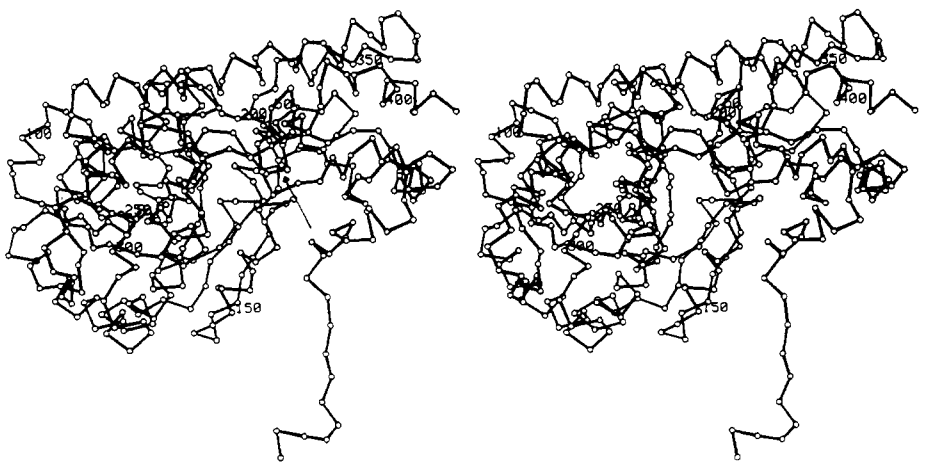

FIGURE 2: Stereoview of the α-carbon trace of the monomer of the K258A mutant of *E. coli* AATase. The view is close to the orientation of the subunit in the dimer. The long helix connecting the small and large domains (see text) is clearly visible on the top edge of the molecule. The N-terminal domain, which interacts with the other subunit in the dimer, is visible at the lower right. The active site is indicated by the arrow.

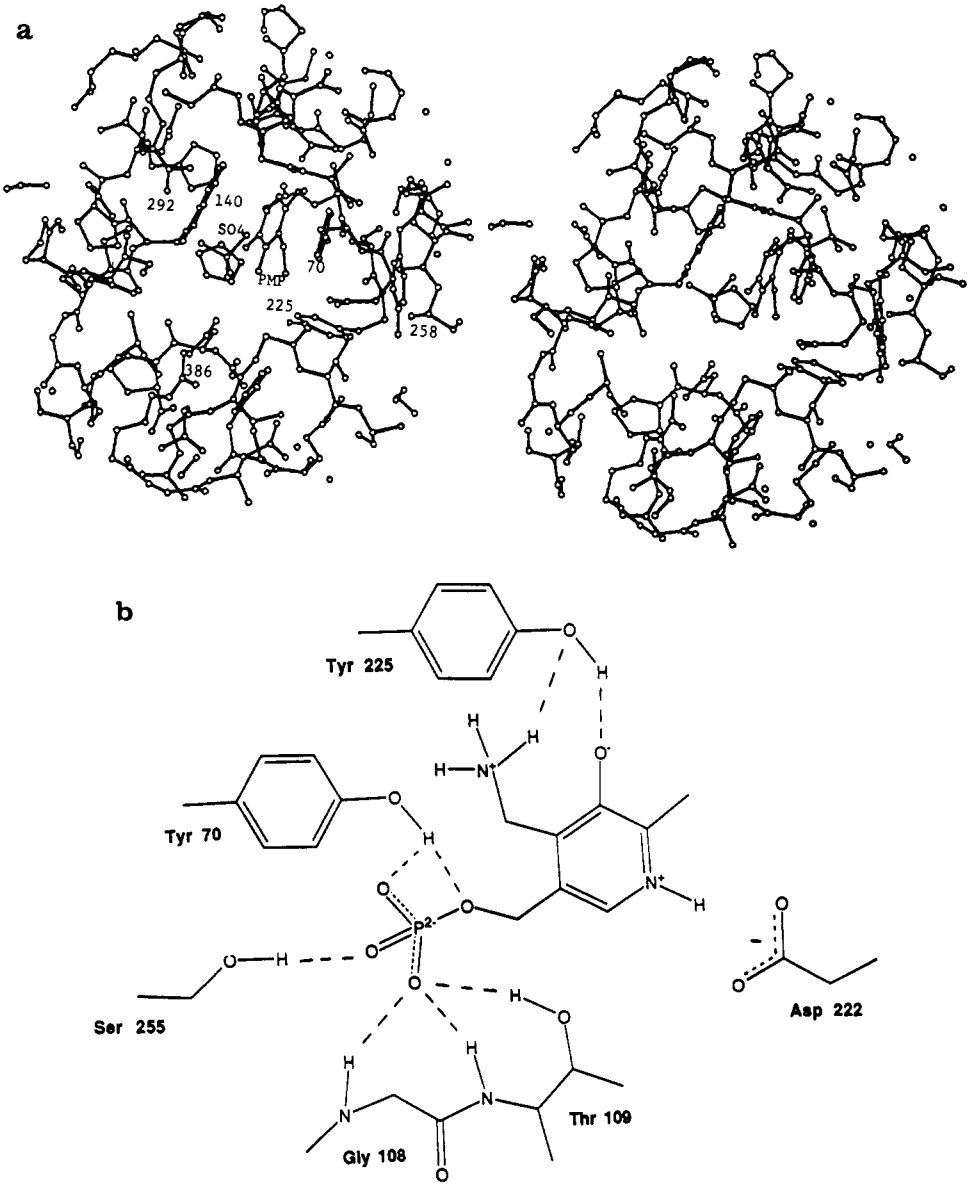

FIGURE 3: (a) Stereoview of the active-site region of the K258A mutant of *E. coli* AATase. The view is into the active site from the interface between the two subunits. Some of the important residues discussed in the text are indicated: Ala 258, Trp 140, Tyr 225, and Arg 386 are from the subunit in which the PMP is bound; Arg 292 and Tyr 70 are from the other subunit. (b) Schematic diagram of the hydrogen-bonding and salt bridge interactions between the PMP cofactor and the surrounding side-chain and main-chain atoms. Trp 140 is not shown because it would be directly on top of the pyridine ring in this view.

Tyr 70 from the other subunit, and Thr 109 and the main-chain NH's of Gly 108 and Thr 109. All of these are observed in the mitochondrial enzyme also. However, the hydrogen bond from the side-chain OH of Ser 107 observed in the mitochondrial AATase structure does not exist in the *E. coli* structure, since this residue is a glycine in the latter enzyme. No other interaction seems to take its place. Finally, the salt bridge between Arg 266 and the phosphate group is conserved in both structures.

The pyridoxyl ring of the PMP cofactor (Figure 4) in the K258A AATase interacts with Asp 222 (via the nitrogen in the ring) and Tyr 225 (via the phenolic hydroxyl group and the amino group of pyridoxamine). This Tyr interacts with the phenolic group of PLP in the mitochondrial enzyme. In addition, the pyridoxyl ring is almost parallel to the indole ring of Trp 140 and lies from 3.3 to 4.5 Å away from it. The angle between the planes of the two rings is ~9°. Both are tipped forward equally (away from the protein) by ~7° relative to the wild-type *E. coli* enzyme, presumably due to the absence of the covalent bond between Lys 258 and the pyridoxal cofactor. This tilt of the cofactor ring in the PMP form relative to the PLP form has been observed for the mitochondrial AATase as well (Jansonius & Vincent, 1987). However, the angle by which the position of the PMP ring differs from the position of the PLP ring in the mitochondrial enzyme is larger (15°). It is possible that the difference in ring tilt between the cofactors of the two enzymes (mitochondrial and *E. coli* mutant) is due to the presence of a sulfate ion in the active site of the *E. coli* mutant structure.

A detailed mechanism for AATase has been described by Kirsch et al. (1984) on the basis of the then unrefined structure of mitochondrial AATase from chicken heart. In this mechanism lysine 258 plays a key role in the initial transaldimination between the substrate (aspartic acid or glutamic acid) and the pyridoxal phosphate–enzyme Schiff base. Once the external aldimine has been formed, lysine is postulated to act as the base involved in the isomerization from aldimine to ketimine. After hydrolysis of the ketimine to give the product keto acid and PMP, lysine 258 presumably could form a hydrogen bond with the amino group of the cofactor. The

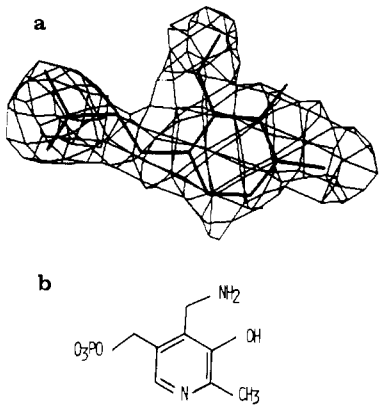

FIGURE 4: (a) Electron density and (b) model of the pyridoxamine phosphate cofactor in the mutant AATase (K258A). The electron density was calculated by using $(2F_o - F_c)\exp\phi_{calc}$ as the Fourier coefficients. The PMP cofactor was omitted from the structure factor calculation, and the density is contoured at 1σ as calculated for the entire protein map.

position of the cofactor in the PMP form would thus be controlled in part by hydrogen-bonding interactions with Lys 258 and Tyr 225. In the K258A mutant none of these interactions with lysine 258 are possible, and thus this enzyme is expected to be inactive toward amino acid substrates because the transaldimination and isomerization cannot be catalyzed. In fact, the PLP form of the mutant has less than 10^{-6} times the activity of the wild-type enzyme toward aspartic acid as a substrate (J. Kirsch, private communication).

In the reverse reaction, the reactivity of the K258A mutant in the PMP form toward keto acids has been observed to give the ketimine, with further progress toward transamination blocked by the absence of the catalytic base. The slower reaction of oxaloacetate toward K258A–PMP relative to wild-type–PMP (J. Kirsch, private communication) suggests that lysine 258 may be involved in positioning the cofactor optimally for reaction with the incoming keto acid and/or stabilizing the unprotonated form of the cofactor amino group. The three-dimensional structure of this mutant supports these ideas about the mechanism of AATase and opens up the possibility of testing them.

ACKNOWLEDGMENTS

We are grateful to G. A. Petsko for use of his equipment and many helpful discussions, to J. Jansonius and G. Eichele for helpful discussions and encouragement and for coordinates of the structure of the mitochondrial enzyme, to J. F. Kirsch for initiating the project with samples of the proteins, and to J. K. Prater and G. Quigley for help on CRAD.

Registry No. AATase, 9000-97-9; PMP, 529-96-4; lysine, 56-87-1; alanine, 56-41-7; tryptophan, 73-22-3.

REFERENCES

Arnone, A., Rogers, P. H., Hyde, C. C., Briley, P. D., Metzler, C. M., & Metzler, D. E. (1985) in *Transaminases* (Christen, P., & Metzler, D. E., Eds.) pp 138–155, Wiley, New York.

Birchmeier, W., Wilson, K. T., & Christen, P. (1973) *J. Biol. Chem. 248*, 1751–1759.

Blow, D. M., & Crick, F. H. C. (1959) *Acta Crystallogr. 12*, 794–802.

Bolon, C., Crawford, J., Deutsch, M., & Quigley, G. (1981) *IEEE Trans. Nucl. Sci. NS28*, 816–820.

Borisov, V. V., Borisova, S. N., Sosfenov, N. I., & Vainshtein, B. K. (1980) *Nature, 284*, 189–190.

Braunstein, A. E. (1973) *Enzymes (3rd Ed.) 9*, 379–481.

Braunstein, A. E., & Kritzman, M. G. (1937) *Nature 140*, 503–504.

Brünger, A. (1988) *J. Mol. Biol. 203*, 803–816.

Brünger, A. T., Kuriyan, J., & Karplus, M. (1987) *Science 235*, 458–460.

Cooper, A. J. L., & Meister, A. (1985) in *Transaminases* (Christen, P., & Metzler, D. E., Eds.) pp 396–412, Wiley, New York.

Dodson, E., & Vijayan, M. (1971) *Acta Crystallogr. B27*, 2402–2411.

Ford, G. C., Eichele, G., & Jansonius, J. N. (1980) *Proc. Natl. Acad. Sci. U.S.A. 77*, 2559–2563.

Gehring, H., & Christen, P. (1978) *J. Mol. Biol. 253*, 3158–3163.

Germain, G., Main, P., & Woolfson, M. M. (1971) *Acta Crystallogr. A27*, 368–376.

Harutyunyan, E. G., Malashkevich, V. N., Tersyan, S. S., Kochkima, V. M., Torchinsky, T. M., & Braunstein, A. E. (1982) *FEBS Lett. 138*, 113–116.

Hendrickson, W. A., & Konnert, J. H. (1980) in *Biomolecular Structure, Function, Conformation, and Evolution* (Srinivasan, R., Ed.) Vol. 1, pp 43–57, Pergamon Press, Oxford, U.K.

Jansonius, J. N., & Vincent, M. G. (1987) in *Biological Macromolecules and Assemblies* (Jurnak, F., & McPherson, A., Eds.) Vol. 3, pp 187–285, Wiley, New York.

Jansonius, J. N., Eichele, G., Ford, G. C., Picot, D., Thaller, C., & Vincent, M. G. (1985) in *Transaminases* (Christen, P., & Metzler, D. E., Eds.) pp 110–138, Wiley, New York.

John, R. A., & Fowler, . J. (1985) in *Transaminases* (Christen, P., & Metzler, D. E., Eds.) pp 413–430, Wiley, New York.

Jones, T. A. (1982) in *Computational Crystallography* (Sayre, D., Ed.) pp 303–317, Clarendon Press, Oxford, U.K.

Jones, T. A., & Thirup, S. (1986) *EMBO J. 5*, 819–822.

Kamitori, S., Hirotsu, K., Higuchi, T., Kondo, K., Inoue, K., Kuramitsu, S., Kagamiyama, H., Higuchi, Y., Yasuoka, N., Kusunoki, M., & Matsuura, Y. (1987) *J. Biochem. 101*, 813–816.

Kiick, D. M., & Cook, P. F. (1983) *Biochemistry 22*, 375–382.

Kirsch, J. F., Eichele, G., Ford, G. C., Vincent, M. G., Jansonius, J. N., Gehring, H., & Christen, P. (1984) *J. Mol. Biol. 174*, 497–525.

Kirsch, J. F., Finlayson, W. L., Toney, M. D., & Cronin, C. N. (1987) in *Biochemistry of Vitamin B_6* (Korpela, T., & Christen, P., Eds.) pp 56–57, Birkhaüser, Basel.

Kondo, K., Wakabayashi, S., Yagi, T., & Kagamiyama, H. (1984) *Biochem. Biophys. Res. Commun. 122*, 62–67.

Malcolm, B. A., & Kirsch, J. F. (1985) *Biochem. Biophys. Res. Commun. 132*, 915–921.

Matthews, B. W. (1968) *J. Mol. Biol. 33*, 491–497.

Metzler, D. E. (1979) *Adv. Enzymol. Relat. Areas Mol. Biol. 50*, 1–40.

Metzler, D. E., & Snell, E. E. (1952) *J. Am. Chem. Soc. 74*, 979–983.

North, A. C. T., Phillips, D. C., & Mathews, F. S. (1968) *Acta Crystallogr. A24*, 351–359.

Sielecki, A. R., Hendrickson, W. A., Broughton, C. G., Delbaere, L. T. J., Brayer, G. D., & James, M. N. G. (1979) *J. Mol. Biol. 134*, 781–804.

Smith, D. L., Ringe, D., Finlayson, W. L., & Kirsch, J. F. (1986) *J. Mol. Biol. 191*, 301–302.

Snell, E. E. (1945) *J. Am. Chem. Soc. 67*, 194–197.
Terwilliger, T. C., & Eisenberg, D. (1983) *Acta Crystallogr. A39*, 813–817.
Torchinsky, Yu. M., Harutyunyan, E. G., Malashkevich, V. N., Kochkina, V. M., Makarov, V. L., & Braunstein, A. E. (1982) *Cell Function and Differentiation, Proceedings of the Special FEBS Meeting, 1982* (Evangelopoulos, A. E., Ed.) Part C, Liss, New York.
Velick, S. F., & Vavara, J. (1962) *J. Biol. Chem. 237*, 2109–2122.
Wang, B.-C. (1985) *Methods Enzymol. 115*, 90–112.
Wyckoff, H. W. (1985) *Methods Enzymol. 114*, 330–385.

Mutations at the Interdomain Hinge Region of the DadB Alanine Racemase: Effects of Length and Conformational Constraint of the Linker Sequence on Catalytic Efficiency†

Nicholas G. Galakatos‡ and Christopher T. Walsh*
Department of Biological Chemistry and Molecular Pharmacology, Harvard Medical School, Boston, Massachusetts 02115
Received March 21, 1989; Revised Manuscript Received June 2, 1989

ABSTRACT: The pentapeptide "hinge" region of the DadB alanine racemase links two structural domains of the protein [Galakatos, N. G., & Walsh, C. T. (1987) *Biochemistry 26*, 8475]. The presence of substrate markedly reduces the rate of hinge-specific proteolysis of this racemase and induces a conformational change observed by circular dichroism. To evaluate the possible contribution of the proteolytically sensitive hinge residues (-Y^{253}GGGY^{257}-) on catalytic efficiency, site-directed mutations were generated to probe the effects of size and conformational rigidity of that region. A bacterial overproducing system for the *dadB* gene was constructed that expresses the enzyme as 4.5% of total soluble protein. On this construct, a four-part ligation allowed the engineering of two unique and proximal restriction sites required for cassette mutagenesis at the hinge region. For two of the eight mutants generated, expressed protein could not be detected (deletion of -GGGY-; termination codon at position 255). Deletion of one or two of the three Gly residues had no effect on catalytic efficiency. Insertion of a fourth Gly resulted in a 5-fold drop in V_{max}/K_m. For G254P, G255P, and G256P, V_{max}/K_m was 60%, 126%, and 26% of the native enzyme, respectively. In all cases, the K_m's remained essentially constant, suggesting that the hinge region is not involved in substrate binding. The rate of hinge-specific proteolysis of the mutants was faster than that of wild-type DadB except for the G255P protein for which it was equivalent.

It has been demonstrated that on average 26% of protein primary sequences are situated in loop regions (Leszcynski & Rose, 1986). For loops found in immunoglobulins and DNA-binding proteins, clear functional significance in recognition and binding has been assigned (Thornton et al., 1988). For enzymes, however, the role of particular loops in the control of catalytic efficiency or specificity is much less known. Surface, flexible portions of the polypeptide chain have recently been implicated in substrate or cofactor binding and as pivot areas for closure of interdomain active-site clefts (Huber, 1988). However, little direct experimental evidence has existed to support these hypotheses.

In some cases, site-directed mutagenesis has met with great success in elucidating aspects of the formidable catalytic efficiency of enzyme species (Knowles, 1987). Most of that work to date has targeted residues at the densely packed active-site region, which appears deceptively rigid. However, many enzyme proteins undergo ligand-induced conformational isomerizations, and thus effects of single-residue alterations can be masked by overall protein dynamics.

Bacterial alanine racemases catalyze the first committed step of peptidoglycan assembly in cell wall biosynthesis and have been of great interest mechanistically and therapeutically (Walsh et al., 1985). Previous work from these laboratories described the cloning, sequence determination, and purification from *Salmonella typhimurium* of two isoenzymic alanine racemases (Wasserman et al., 1984; Galakatos et al., 1986), one with a low k_{cat} (*alr* gene encoded) and the other (*dadB* gene encoded) with a 20–60-fold higher k_{cat} (Esaki & Walsh, 1986). Also reported is the analysis of the reaction profile energetics and the mechanism of inactivation of these PLP[1]-dependent racemases by natural and synthetic antibacterial agents (Faraci & Walsh, 1988).

The *S. typhimurium* racemases have so far proven refractory to crystallization, so in initial structure–function studies we have reported on the limited proteolysis of the DadB alanine racemase (Galakatos & Walsh, 1987). DadB was shown to possess a protease-labile loop region that connects two structural domains and is conserved in all four alanine racemase sequences reported from both Gram-negative and Gram-positive organisms. Proteolytic removal of the intraloop tetrapeptide -G^{254}GGY^{257}- from the 356-residue monomeric protein generates an enzyme species in which the two fragments remain associated. This "clipped" protein retains its

† This work was supported in part by a grant from the National Science Foundation (PCM 8308969).
* To whom correspondence should be addressed.
‡ Present address: CIBA-GEIGY Corp., Pharma Division, Summit, NJ 07901.

[1] Abbreviations: CIP, calf intestinal alkaline phosphatase; dNTP, deoxynucleotide triphosphate; IPTG, isopropyl β-D-thiogalactopyranoside; X-Gal, 5-bromo-4-chloro-3-indolyl β-D-galactopyranoside; DMT, 4′,4′-dimethoxytrityl; PLP, pyridoxal 5′-phosphate; SDS, sodium dodecyl sulfate; CHES, 2-(*N*-cyclohexylamino)ethanesulfonic acid; Tris, tris(hydroxymethyl)aminomethane; EDTA, ethylenediaminetetraacetic acid; kb, kilobase; bp, base pair(s); Δ, residue deletion.

0006-2960/89/0428-8167$01.50/0